Imaging, Diagnosis, Prognosis

Clinical Cancer Research

Measurement of Tumor VEGF-A Levels with ^{89}Zr-Bevacizumab PET as an Early Biomarker for the Antiangiogenic Effect of Everolimus Treatment in an Ovarian Cancer Xenograft Model

Arne R.M. van der Bilt[1,2], Anton G.T. Terwisscha van Scheltinga[1,3], Hetty Timmer-Bosscha[1], Carolien P. Schröder[1], Linda Pot[1], Jos G.W. Kosterink[3], Ate G.J. van der Zee[2], Marjolijn N. Lub-de Hooge[3,4], Steven de Jong[1], Elisabeth G.E. de Vries[1], and Anna K.L. Reyners[1]

Abstract

Purpose: The mTOR pathway is frequently activated in ovarian cancers. mTOR inhibitors, such as everolimus, can reduce VEGF-A production by cancer cells. We investigated whether early everolimus treatment effects could be monitored by positron emission tomography (PET) with ^{89}Zr-bevacizumab.

Experimental Design: The effect of everolimus on VEGF-A secretion was determined in a panel of human ovarian cancer cell lines and in A2780^{luc+} ovarian cancer cells xenografted subcutaneously in BALB/c mice. Mice received daily 10 mg/kg everolimus intraperitoneally (i.p.) for 14 days. PET scans with the tracer ^{89}Zr-labeled bevacizumab were conducted before and after treatment. *Ex vivo* ^{89}Zr-bevacizumab biodistribution and correlative tissue analyses were conducted. Tumor VEGF-A levels were measured with ELISA and mean vascular density (MVD) was determined with immunohistochemistry.

Results: Everolimus treatment reduced VEGF-A levels in the supernatant of all cell lines. Everolimus lowered ^{89}Zr-bevacizumab tumor uptake by 21.7% ± 4.0% [mean standardized uptake value (SUV_{mean}) 2.3 ± 0.2 vs. 2.9 ± 0.2, $P < 0.01$]. *Ex vivo* biodistribution also showed lower tracer uptake in the tumors of treated as compared with control animals (7.8 ± 0.8%ID/g vs. 14.0 ± 1.7%ID/g, $P < 0.01$), whereas no differences were observed for other tissues. This coincided with lower VEGF-A protein levels in tumor lysates in treated versus untreated tumors ($P = 0.04$) and reduced MVD ($P < 0.01$).

Conclusion: Tumor VEGF-A levels are decreased by everolimus. ^{89}Zr-bevacizumab PET could be used to monitor tumor VEGF-A levels as an early biomarker of the antiangiogenic effect of mTOR inhibitor therapy. *Clin Cancer Res; 18(22); 6306–14. ©2012 AACR.*

Introduction

Patients with ovarian cancer often present with advanced stage disease and develop resistance to conventional (platinum-based) chemotherapy during the course of treatment, resulting in a poor 30% 5-year survival rate (1). To improve ovarian cancer prognosis, there is a clear need for additional therapeutic options. Because ovarian cancers are often extensively vascularized and overexpress proangiogenic factors, such as VEGF-A, angiogenesis inhibition has been studied as a therapeutic strategy. Phase II and III trials with the VEGF-A–neutralizing antibody bevacizumab or with VEGF receptor (VEGFR)–targeted tyrosine kinase inhibitors (TKI) targeting vascular endothelial cells have shown antitumor activity in a subgroup of patients (2, 3).

The kinase mTOR is a potential alternative target for antiangiogenic therapy. The mTOR pathway is activated in 64% to 85% of ovarian cancers (4, 5). mTOR enhances translational efficacy of mRNAs that contain intricate 5′-untranslated regions (5′-UTR). These regions encode oncogenic proteins, such as hypoxia-inducible factor (HIF) and VEGF-A (6, 7). By reducing the synthesis of these proteins by tumor cells, mTOR inhibitors have distinct antiangiogenic effects as compared with classical antiangiogenic drugs, such as bevacizumab (8).

In transgenic (orthotopic) and xenograft mouse models, treatment with the mTOR inhibitor everolimus delayed tumor development, reduced tumor burden, and prolonged

Authors' Affiliations: Departments of [1]Medical Oncology, [2]Gynecological Oncology, [3]Hospital and Clinical Pharmacy, and [4]Nuclear Medicine and Molecular Imaging, University of Groningen, University Medical Center Groningen, Groningen, The Netherlands

Note: Supplementary data for this article are available at Clinical Cancer Research Online (http://clincancerres.aacrjournals.org/).

A.R.M. van der Bilt and A.G.T. Terwisscha van Scheltinga contributed equally to this work.

Corresponding Author: Anna K.L. Reyners, Department of Medical Oncology, University of Groningen, University Medical Center Groningen, Hanzeplein 1, 9713 GZ Groningen, The Netherlands. Phone: 31-50-3611543; Fax: 31-50-3614862; E-mail: a.k.l.reyners@umcg.nl

doi: 10.1158/1078-0432.CCR-12-0406

Translational Relevance

The mTOR is frequently activated in ovarian cancers and is involved in tumor angiogenesis. Drugs inhibiting mTOR are of interest as they can exert antitumor activity, which is in part executed by reducing VEGF-A production. Clinical studies indicate benefit of mTOR inhibition in a subgroup of patients with ovarian cancer, but biomarkers for patient selection are currently lacking. Our data show that ^{89}Zr-bevacizumab positron emission tomography (PET) provides a novel tool for noninvasive monitoring of antiangiogenic effects upon mTOR inhibitor therapy. These results support the evaluation of measuring tumor VEGF-A levels with ^{89}Zr-bevacizumab PET as an early biomarker for the antiangiogenic effect of mTOR inhibitors in clinical studies.

survival (9–12). mTOR inhibition reduced VEGF-A expression and diminished vascularization in murine (xenograft) ovarian cancers (9, 10). This was even more pronounced when combined with bevacizumab (13).

In a phase II trial, 60 patients with persistent or recurrent ovarian cancer received weekly temsirolimus (14). A partial tumor response was observed in 9.3% of the patients, with disease stabilization in a further 40.7% (14). This underscores the importance of discovering biomarkers for upfront patient selection or early response prediction. However, no biomarkers are currently established for predicting everolimus or VEGF(R)-targeted drug efficacy in ovarian cancer.

Whole-body positron emission tomography (PET) can potentially address this issue. It offers the possibility for longitudinal *in vivo* monitoring of tumor biology and changes herein upon treatment. To visualize antiangiogenic drug efficacy, we generated radiolabeled bevacizumab, which proved capable of noninvasively detecting tumor VEGF-A levels in animal models and patients (15–17).

The aim of this study was to analyze the effect of everolimus on ovarian cancer VEGF-A secretion *in vitro* and *in vivo*, and the potential of serially measuring tumor VEGF-A levels with ^{89}Zr-bevacizumab PET as an early predictive biomarker for everolimus antiangiogenic efficacy in an ovarian cancer xenograft model.

Materials and Methods

Cell lines

The human ovarian cancer cell line A2780 was kindly provided by Dr. T.C. Hamilton (Fox Chase Cancer Center, Philadelphia, PA). The luciferase-transfected subline A2780^{luc+} was developed as described earlier (18). SKOV-3 and TOV-21G ovarian cancer cell lines were obtained from the American Type Culture Collection. A2780 and A2780^{luc+} cells were cultured in RPMI-1640, supplemented with 10% fetal calf serum (FCS, Bodinco BV) and 2 mmol/L L-glutamine (Invitrogen), SKOV-3 in Dulbecco's modified Eagle's medium (DMEM) with 4.5 g/L glucose, supplemented with 10% FCS, and TOV-21G cells in Ham-F12 and DMEM (1:1), supplemented with 10% FCS. All culture media were purchased from Invitrogen. All cell lines were cultured at 37°C in a fully humidified atmosphere containing 5% CO_2.

For *in vitro* experiments, cells were harvested with trypsin after a single wash with PBS (6.4 mmol/L Na_2HPO_4, 1.5 mmol/L KH_2PO_4, 0.14 mmol/L NaCl, 2.7 mmol/L KCl, pH 7.2) and seeded in 6-well plates (A2780: 31,500 cells/cm^2, SKOV-3: 21,000 cells/cm^2, TOV-21G: 52,500 cells/cm^2). The next day, everolimus was added in fresh medium (1.5 mL/well) to reach final concentrations of 0 to 100 nmol/L.

Compounds

Everolimus was obtained from LC Laboratories (E-4040, stored at −20°C). For *in vitro* use, everolimus was dissolved in dimethyl sulfoxide (DMSO) at 10 mmol/L stock concentration stored at −20°C. For *in vivo* use, everolimus was dissolved in DMSO and formulated in a stable suspension with PBS containing 0.5% Tween-80 (Sigma-Aldrich). Mice received 10 mg/kg everolimus daily via intraperitoneal injection (10 mL/kg). The everolimus dosage used is based on previous efficacy studies in xenografted mice, in which 5 to 10 mg/kg daily resulted in unbound (active) everolimus plasma levels comparable with those reached in humans receiving 5 to 10 mg daily due to higher plasma protein binding and shorter $T_{1/2}$ values in mice (8, 19–22).

Western blotting

Total and phosphorylated protein expression of mTOR target proteins was measured by Western blotting. After 24 hours of everolimus exposure, adherent cell layers were washed 3 times with ice-cold PBS, and total cellular protein content was extracted with mammalian protein extraction reagent (M-PER, Thermo Scientific). Protease and phosphatase inhibitors (Thermo Scientific) were added (1:100). Protein yield was determined with the Bradford assay (23). Samples were diluted 1:1 with SDS sample buffer, containing 125 mmol/L Tris–HCl, 2% SDS, 10% glycerol, 0.001% bromophenol blue, and 10% β-mercaptoethanol, and boiled for 5 to 10 minutes before storage at −20°C. Proteins (20–30 μg) were separated on SDS-PAGE and transferred onto polyvinylidene difluoride (PVDF) membranes (Immobilon-P, Millipore) by wet blotting (24). Primary antibodies were purchased from Cell Signaling, recognizing epitopes on p70S6K (#2708), phosho-p70S6K (Thr389; #9206), S6 (#2217), phospho-S6 (Ser235/236; #4856), 4E-BP1 (#9644), and phospho-4E-BP1 (Thr70; #9455). Anti–β-actin antibody (BP Biomedicals) served to assure equal protein loading. Membranes were incubated with horseradish peroxidase (HRP)–labeled secondary antibodies (DAKO) for 1 hour at room temperature. Protein bands were visualized with chemiluminescence using Lumi-Light^{plus} (Roche Diagnostics).

VEGF-A ELISA

After 24 hours incubation with everolimus, cell culture supernatant was removed and centrifuged for 10 to 15 minutes at 450 × *g*, to remove any residual cells or cell remnants, and subsequently stored in aliquots at −20°C until VEGF-A levels were measured with VEGF Quantikine ELISA kits (DVE00, R&D Systems). To correct for experimental differences, cell counting was conducted in parallel for each sample using conventional counting grids and Trypan blue staining.

For *in vivo* studies, 3 random cores were die-cut from frozen tumor samples and lysed using M-PER (16). In these whole-tumor protein lysates, VEGF-A levels were assayed with ELISA kits and total protein content with Bradford assays as described earlier.

Xenograft model

All animal experiments were approved by the Institutional Animal Care and Use Committee of the University of Groningen (Groningen, The Netherlands). Animal studies were conducted in male nude BALB/c mice (BALB/cOlaHsd-*Foxn1*^{nu}, Harlan). Animals were allowed to feed *ad libitum*. Experiments were carried out under isoflurane inhalation anesthesia (induction 3%, maintenance 1.5%).

Mice ($n = 10$) were xenografted subcutaneously in the flank with 5×10^6 A2780^{luc+} cells resuspended in 0.3 mL of a 1:1 mixture of PBS and Matrigel (BD Biosciences). To ensure tumor viability, bioluminescence imaging was conducted using the IVIS Spectrum system (Caliper Life Sciences). D-luciferin (150 mg/kg, purchased from Xenogen) was reconstituted in PBS and injected intraperitoneally 20 minutes before image acquisition. Twelve days after tumor inoculation, when the tumor diameter measured 6 to 8 mm (~300 mm^3), a baseline 6-day microPET scan sequence was conducted to determine pretreatment ^{89}Zr-bevacizumab tracer uptake (Supplementary Fig. S1). Daily everolimus treatment [10 mg/kg intraperitoneal (i.p.) administration] was started immediately after completing the baseline scan sequence and continued for 14 days. On day 9, during everolimus treatment, a second 6-day scan sequence was initiated after ^{89}Zr-bevacizumab injection. Animals that received everolimus were sacrificed immediately after acquiring the posttreatment scans.

To allow comparison between treated versus untreated tumors, a separate group of mice ($n = 5$, control group) was sacrificed after the baseline scans. Mice xenografted with A2780^{luc+} cells develop rapidly growing tumors, with a doubling time of 3 to 6 days (16). Therefore, control animals cannot be maintained for the same duration as the treatment group, as tumors will grow beyond tolerable sizes. To obtain data on tumor volumes, regular caliper measurements were conducted as described previously (17). Tumor growth curves were related to control data from untreated A2780^{luc+} tumor-bearing mice obtained earlier (17).

MicroPET imaging

Bevacizumab conjugation and labeling were conducted as described previously (15). Briefly, quality controls included size-exclusion high-performance liquid chromatography (SE-HPLC), trichloroacetic acid (TCA) precipitation, and immunoreactivity analysis. Radiochemical purity of all injected tracers was more than 95%. ^{89}Zr-bevacizumab (±5 MBq, ±30 μg) was injected into the penile vein. Animals were imaged using a microPET Focus 220 rodent scanner (CTI/Siemens). Static images were obtained (15–45 minutes acquisition) immediately after tracer injection and at 144 hours after tracer injection. In earlier tracer validation studies, it was shown that the ^{89}Zr-bevacizumab tumor uptake was significantly higher as compared with ^{89}Zr-IgG uptake, showing target-driven, tumor-specific binding and accumulation of the tracer (15, 16). ^{89}Zr-bevacizumab tumor uptake is optimal in this animal model at 144 hours after tracer injection (15, 16). The tracer dose was also based on these tracer validation studies (25). At this tracer dose, any retained cold antibody from the first tracer injection is not expected to influence tumor uptake at the second scanning period. Images were analyzed and quantified using AMIDE software [version 0.9.1, Stanford University (Stanford, CA); ref. 26]. Imaging data are presented as the mean standardized uptake value (SUV_{mean}; ref. 17).

Biodistribution

Organs and tissues were excised, rinsed of residual blood, and weighed. Tissues were counted for radioactivity in a calibrated well-type LKB-1282-Compu-gamma system (LKB Wallac), together with reference tracer material to correct for physical decay. *Ex vivo* tissue activity is expressed as the percentage of the injected dose per gram of tissue (%ID/g). Harvested tumors were divided, and partly paraffin-embedded and partly frozen at −80°C for further *ex vivo* analysis.

Immunohistochemistry

Slices (3 μm thick) were cut from paraffin-embedded tumor sections using a microtome and placed on 3-aminopropyltriethoxysilane–coated glass slides. Heat-induced antigen retrieval was conducted in 10 mmol/L citrate buffer (S6, p-S6) or Tris/EDTA (Ki67) using a 400 W rotary microwave, or by using Proteinase K [Von Willebrand factor (vWF)] at room temperature. Endogenous peroxidase was blocked by 30 minutes incubation with 0.3% H_2O_2 in PBS. Endogenous avidin/biotin activity was blocked using a commercially available blocking kit (Vector Laboratories). Slides were incubated with primary antibodies detecting human S6 and p-S6 (Cell Signaling, #2217 and #2211) and Ki67 (Dako, 1:350). In addition, slides were stained with anti-vWF antibody (Dako, 1:250) to determine the mean vascular density (MVD; ref. 17). Staining was visualized after incubation with biotinylated or peroxidase-bound secondary antibodies (Dako) using, when necessary, the streptavidin–biotin/HRP complex (Dako) and 3,3′-diaminobenzidine (DAB; Sigma-Aldrich). Hematoxylin counterstaining was applied routinely and hematoxylin and eosin (H&E) staining served to analyze tissue viability and morphology.

Stainings were quantified by evaluation of 10 high-power fields (HPF; ×400 magnification) using a calibrated grid, counting positive and negative cells (S6 and p-S6, cytoplasmic staining) or nuclei (Ki67). Data are expressed as the percentage of positive cells. MVD was determined by counting and averaging the number of vessels within 10 HPFs. Photographs were acquired by digitalized scanning of slides using the NanoZoomer 2.0-HT multi-slide scanner (Hamamatsu). To calculate tumor viability, acquired images from H&E-stained slides were analyzed using NanoZoomer Digital Pathology (NDP) viewer software (Hamamatsu). Using the freehand surface area tool, areas with nonviable tumor tissue were delineated within fixed-size squares overlaying the surface area of the slide.

Statistical analyses

Data are presented as mean ± SD. For *in vitro* experiments, different experimental conditions were compared using unpaired Student *t* tests. Comparison of ^{89}Zr-bevacizumab uptake before and after everolimus treatment was conducted using the paired *t* test, whereas unpaired testing was used for *ex vivo* analyses (comparing control vs. treatment group data). Correlations were determined by Pearson correlation coefficient. Statistical analyses were conducted using Prism v.5 (GraphPad). A *P* value of less than 0.05 (two-tailed) was considered significant.

Results

mTOR inhibition by everolimus reduces ovarian cancer VEGF-A secretion *in vitro*

Target inhibition by everolimus was shown by reduced phosphorylation of p70S6K, S6, and 4E-BP1 in all cell lines tested (Fig. 1A). mTOR inhibition occurred within 2 hours upon everolimus exposure (Fig. 1B).

Everolimus reduced VEGF-A secretion by all cell lines ($P < 0.05$ at all concentrations used, compared with untreated controls; Fig. 2). The maximum effect was achieved at relatively low concentrations of everolimus (10 nmol/L). After 24 hours of drug exposure, VEGF-A levels in the culture supernatant were reduced by 57% ± 7% in A2780, 42% ± 15% in SKOV-3, and 38% ± 3% in TOV-21G cells as compared with untreated cells. Cell counting experiments revealed no effect on cell number or viability after 24 hours everolimus incubation.

Everolimus reduces ^{89}Zr-bevacizumab tumor uptake in xenografted mice

^{89}Zr-bevacizumab tracer uptake was homogeneously present within the tumors analyzed at each timepoint based on microPET scans. Everolimus decreased ^{89}Zr-bevacizumab tumor uptake compared with pretreatment (baseline) scans in all animals. Figure 3A shows representative PET images. In pretreatment scans, the SUV_{mean} was 2.9 ± 0.2,

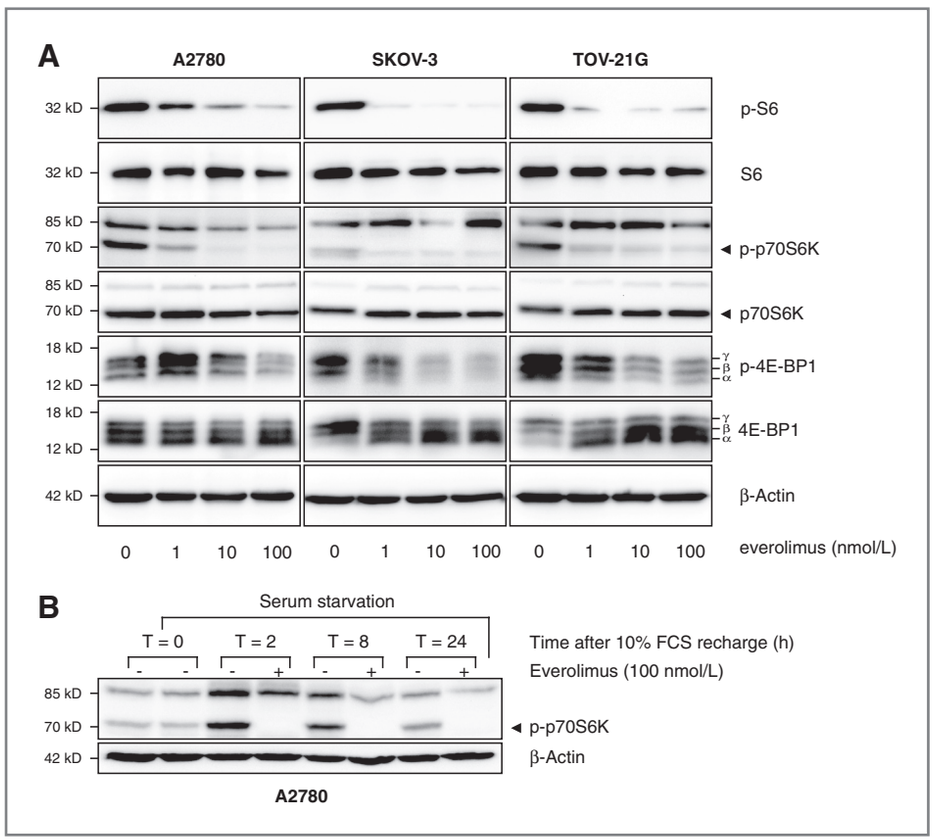

Figure 1. A, A2780, SKOV-3, and TOV-21G cells were treated for 24 hours with everolimus at the indicated concentrations. Western blotting showed that phosphorylation of downstream mTOR target proteins S6, p70S6K, and 4E-BP1 was effectively reduced in all cell lines at all concentrations used. The upper band in the (p-) p70S6K blots is a consequence of analogous binding to p85S6K, which is another S6K splice variant. The α, β, and γ isoforms of 4E-BP1 reflect differential phosphorylation, with the γ-isoform being most extensively phosphorylated. β-Actin was used as a loading control. B, A2780 cells were serum-starved overnight before everolimus (100 nmol/L) was added to the culture medium. After 30 minutes of preincubation with everolimus, FCS was added for the indicated timepoints. As shown by the lack of p70S6K phosphorylation, mTOR is already inhibited shortly after drug exposure and inhibition persisted throughout the whole incubation period.

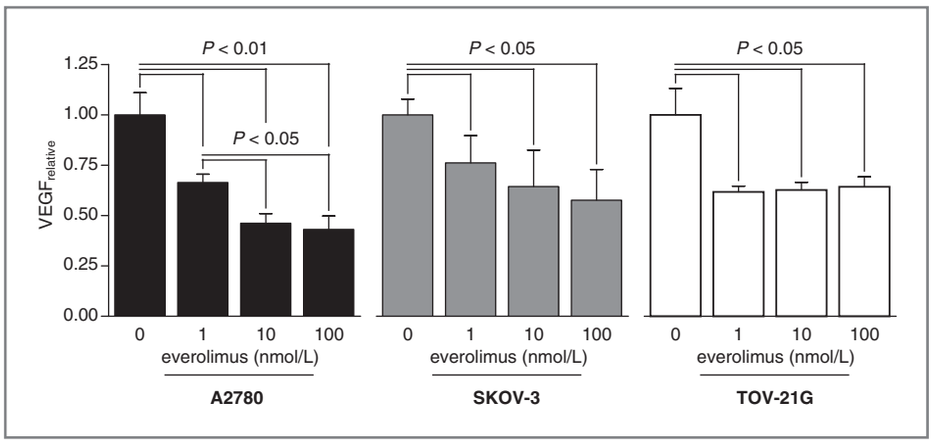

Figure 2. Everolimus reduces VEGF-A secretion in a panel of 3 ovarian cancer cell lines. Cells were exposed for 24 hours at the indicated concentrations of everolimus. VEGF-A levels (measured in pg/mL supernatant) are expressed relative to those measured in the supernatant of untreated cells, corrected for cell number. VEGF-A levels were lower at all concentrations used ($P < 0.05$).

compared with 2.3 ± 0.2 in posttreatment scans after 2 weeks of everolimus treatment (21.7% ± 4.0% decrease in tracer uptake, $P = 0.0005$; Fig. 3B).

Analogous, *ex vivo* biodistribution experiments showed a lower ^{89}Zr-bevacizumab tumor uptake in everolimus-treated animals versus control animals (7.8 ± 0.8%ID/g vs. 14.0 ± 1.7%ID/g, $P < 0.01$; Fig. 3C). These results correlated with microPET quantification data ($R^2 = 0.93$, $P < 0.0001$). No differences in ^{89}Zr-bevacizumab uptake were observed for nontumor tissues between treated and untreated animals (Fig. 3D).

During the 14-day treatment period, tumor volumes in mice receiving everolimus increased to a maximum of 135% ± 17% as compared with the start of treatment (Fig. 4). Tumor growth during everolimus treatment was slower as compared with historical controls (untreated A2780^{luc+} xenograft-bearing mice), which showed a similar increase in tumor volume already at day 3 after baseline scans (17).

Decreased ^{89}Zr-bevacizumab tumor uptake corresponds with reduced tumor VEGF-A levels and reduced vascularity after everolimus treatment

Everolimus treatment resulted in effective target inhibition as the expression of phosphorylated S6 was clearly reduced in treated tumors versus tumors obtained from control animals after baseline scanning, whereas total S6 expression was not affected (Fig. 5A). Morphologic analysis of H&E-stained slides revealed no difference in tumor viability between treated and control tumors (Fig. 5B). After 2 weeks of everolimus treatment, the Ki67-based proliferation index was lower in treated (30.21% ± 1.76%) as compared with control tumors (50.86% ± 1.46%, $P < 0.0001$; Fig. 5C).

VEGF-A protein expression was lower in everolimus-treated versus control tumors (0.33 ± 0.02 vs. 0.50 ± 0.16 pg/μg total protein, $P = 0.04$; Fig. 5D). In addition, everolimus treatment reduced tumor vascularity, as the MVD averaged 4.1 ± 1.4 in treated versus 7.8 ± 1.4 vessels per HPF ($P < 0.01$) in control mice (Fig. 5E). VEGF-A protein levels correlated with microPET quantification data ($R^2 = 0.43$, $P < 0.05$) and *ex vivo* biodistribution data ($R^2 = 0.44$, $P < 0.05$).

Discussion

This study shows that *in vivo* serial ^{89}Zr-bevacizumab PET imaging can visualize reduced tumor VEGF-A levels upon treatment with everolimus in an ovarian cancer xenograft model.

The relatively modest activity of temsirolimus observed in patients with ovarian cancer underscores the need for patient selection. Responses limited to a subset of patients with ovarian cancer have also been observed with VEGF(R)-targeted antiangiogenic drugs, as well as several other targeted agents, and could result from marked molecular heterogeneity, which is characteristic to ovarian cancer (27, 28). The discovery of biomarkers for (early) response prediction might permit the selection of patients that are likely to benefit from single-agent mTOR inhibition or mTOR inhibitor-based combination regimens. Several proteins involved in mTOR signaling have been proposed as suitable biomarkers for response. Phosphorylation of mTOR in ovarian cancer specimens is a poor indicator of its kinase activity (5). Phosphorylation of downstream target proteins (e.g., p70S6K, S6, and 4E-BP1) is a better read-out for mTOR activity and has been used to check for effective drug delivery and optimal biologic dosing in phase I clinical trials with everolimus (20, 29). Using these protein expression levels as biomarkers for response is hampered by the need for (repeat) tumor tissue acquisition, or the use of surrogate tissues, such as peripheral blood mononuclear cells, skin, or hair follicles. Instability of phosphorylated proteins further challenges the reliability (and reproducibility) of such analyses (30).

In vivo molecular imaging provides an attractive alternative. It allows for whole-body, noninvasive monitoring of tumor biology, and changes herein resulting from drug administration. These techniques are being explored as tools for patient selection for several molecular-targeted drugs, including mTOR inhibitors. Thus far, [^{18}F]fluoro-2-deoxy-D-glucose PET (FDG-PET) measuring tumor glucose metabolism has received most attention (31, 32). Inhibition of mTOR does indeed reduce glucose uptake by reducing glucose transporter 1 (GLUT1) expression and/or hexokinase activity (33). However, changes in FDG-PET

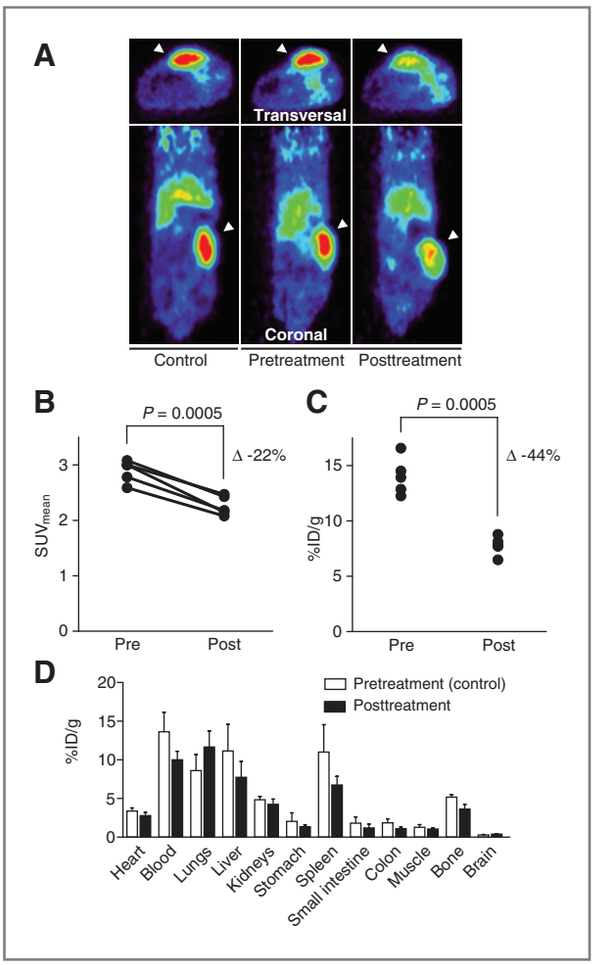

Figure 3. A, representative transversal and coronal ^{89}Zr-bevacizumab microPET images of A2780^{luc+} xenografted mice in the control and treatment group. Pre- and posttreatment images are from the same animal. Tumors are indicated by arrowheads. Scans were acquired with the animals lying sideways with the inoculated left flank upwards. Tracer uptake in the tumor is clearly visible, as well as some aspecific liver uptake. B, microPET quantification in individual everolimus-treated animals showed a clear reduction in the SUV_{mean} as compared with pretreatment scans. A 22% $\pm$ 4.0% decrease in tracer uptake was observed ($P = 0.0005$). C, *ex vivo* biodistribution was conducted in control and treated animals directly after obtaining the final ^{89}Zr-bevacizumab PET scans. Tracer uptake is expressed as percentage of injected dose per gram of tissue (%ID/g). Compared with tumors derived from control animals, everolimus-treated animals show lower tumor uptake by 44% ($P = 0.0005$). D, biodistribution data from nontumor tissues collected from control animals after the baseline scans (pretreatment) and from treated animals after the second scanning sequence (posttreatment). Data are expressed as percentage of the injected dose per gram of tissue (%ID/g).

according to European Organisation for Research and Treatment of Cancer (EORTC) criteria did not correlate with radiographic response according to Response Evaluation Criteria in Solid Tumors (RECIST) criteria or progression-free survival in 34 patients with different cancer types treated with rapamycin (31).

Given the role of mTOR in angiogenesis, we instead monitored the downstream effect of mTOR inhibition by

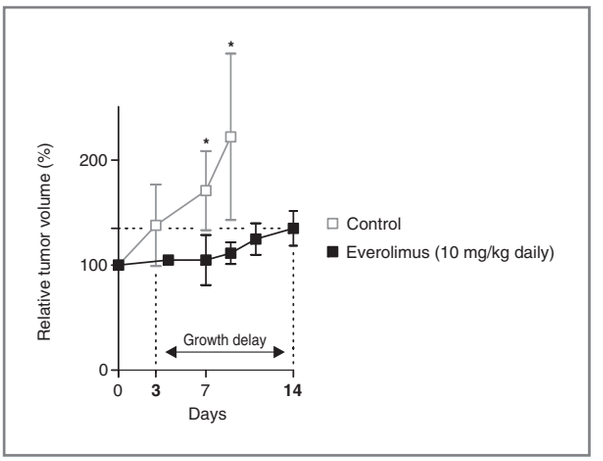

Figure 4. Tumor size determined by caliper measurements in everolimus-treated animals compared with controls (untreated A2780^{luc+} xenograft-bearing mice; ref. 17). The point of reference is set at day 0, the last day of the baseline scanning sequence after which everolimus administration was started. After 7 days of everolimus treatment, the tumors were smaller in treated animals versus controls. Control animals had to be terminated at day 9 because of excessive tumor outgrowth.

everolimus on VEGF-A levels in xenografted ovarian cancers with ^{89}Zr-bevacizumab PET. Everolimus treatment resulted in reduced ^{89}Zr-bevacizumab tumor uptake, which coincided with delayed tumor growth, lower tumor VEGF-A protein expression, and reduced MVD.

Accumulation of radiolabeled bevacizumab results from its interaction with larger human VEGF-A isoforms bound to (tumor) cell surfaces and extracellular matrix components (34). For VEGF-A_{165}, the most abundant isoform, equilibrium is thought to exist between bound and freely diffusible fractions due to weak binding properties. ^{89}Zr-bevacizumab PET thus has the potential of not only visualizing presence but also activity of tumor-associated VEGF-A. This is supported by the finding that there was a 48% reduction in tumor vascularity (MVD) after everolimus treatment, showing an antiangiogenic response. These findings are of interest to evaluate in the clinic. ^{89}Zr-bevacizumab PET is already known to show excellent tracer uptake in tumor lesions of patients with renal cell cancer and is currently tested as an early biomarker for response to everolimus in 2 clinical trials (Everol*image*, NCT01028638; NETPET, NCT01338090; ref. 35). Moreover, ^{89}Zr-bevacizumab PET might provide more insight in differential effects of antiangiogenic drugs on individual tumor lesions within a patient.

It is of interest that we observed a homogeneous decrease in tracer uptake after everolimus treatment based on micro-PET scans. This was also observed previously with the HSP90 inhibitor NVP-AUY922 (16). This differs from previous findings with the VEGFR-targeted TKI sunitinib, which acts at the level of the endothelial cells. ^{89}Zr-ranibizumab, the radiolabeled Fab-fragment derived from bevacizumab, was used to visualize the effect of sunitinib treatment on tumor VEGF-A levels in an ovarian cancer xenograft model (17). Reduction of tracer uptake was more pronounced in the tumor center versus the rim of the tumor.

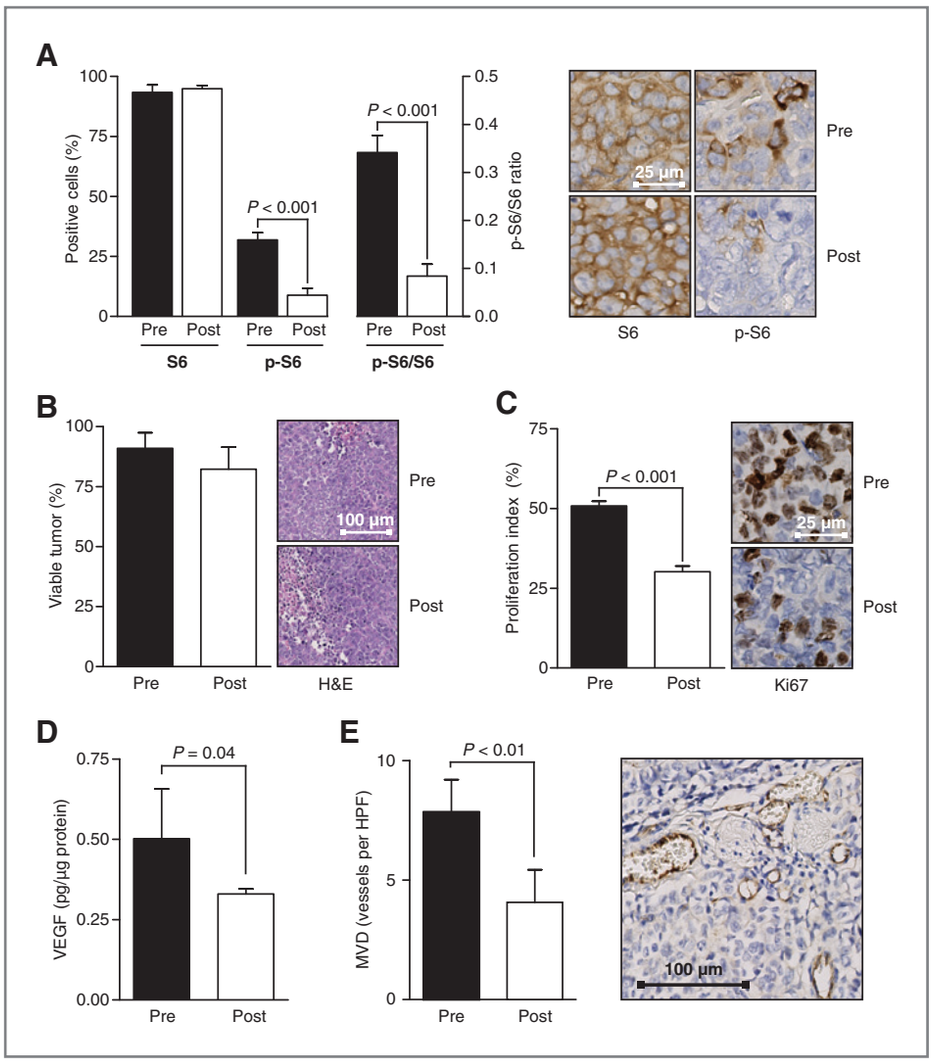

Figure 5. A, S6 expression was homogeneously present in more than 90% of tumor cells, whereas p-S6 was heterogeneously expressed. Everolimus treatment did not change total S6 expression, whereas p-S6 expression was significantly reduced in treated versus control tumors ($P < 0.001$). There was a marked decrease in the ratio between p-S6/S6, which was determined for each individual tumor. B, tumor viability is expressed as the percentage of viable tumor tissue within the total surface area analyzed. No significant differences in tumor viability were observed between treated and control tumors. C, the proliferation index is expressed as the percentage of nuclei positive for Ki67. Compared with control tumors, everolimus treatment reduced the proliferating fraction by 41% ($P < 0.001$). D, VEGF-A levels determined in whole-tumor lysates show reduced VEGF-A in everolimus-treated versus control tumors ($P = 0.04$). VEGF-A levels are expressed relative to the total protein content of each lysate, to correct for loading differences. E, MVD, presented as the average number of vWF-positive vessels per HPF, was reduced in treated versus control tumors (48% decrease, $P < 0.01$). A representative picture is included that shows an angiogenic area in a control tumor, showing specific staining of tumor vasculature.

Increased invasiveness was observed in xenograft models treated with sunitinib, and it was speculated that hypoxia (and consequently HIF activity) drives this adaptive response (36). Lack of differential tracer uptake between tumor center and periphery observed with mTOR or HSP90 inhibitors might reflect their potential to inhibit HIF activity, through reducing its translation or stability.

Our results provide a proof-of-principle of using ^{89}Zr-bevacizumab PET to monitor reduction of tumor VEGF-A levels in response to antiangiogenic treatment with everolimus. The *in vivo* experiments were carried out in a subcutaneous human ovarian cancer xenograft. The sensitivity (resolution) of PET scanning requires a minimum volume and minimum of tracer uptake to detect and quantify any individual tumor lesion. This hampers tumor visualization and quantification of tracer uptake in small tumor lesions, certainly when trying to visualize disseminated disease in the peritoneal cavity of small animals, such as mice. Clinical studies are needed to determine whether this imaging modality would also allow visualization of VEGF-A levels in patients with widespread disseminated, intraperitoneal disease.

Collectively, our data show that ^{89}Zr-bevacizumab PET provides a novel tool for noninvasive monitoring of antiangiogenic effects upon mTOR inhibitor therapy. It provides an interesting candidate biomarker in cancers in which angiogenesis inhibition is thought to underlie treatment efficacy, such as ovarian cancer. Our results support the evaluation of ^{89}Zr-bevacizumab PET to measure tumor VEGF-A levels as an early biomarker for antiangiogenic efficacy of mTOR inhibitor therapy in clinical studies.

Disclosure of Potential Conflicts of Interest

No potential conflicts of interest were disclosed.

Authors' Contributions

Conception and design: A.R.M. van der Bilt, A.G.T. Terwisscha van Scheltinga, C.P. Schröder, J.G.W. Kosterink, M.N. Lub-de Hooge, S. de Jong, E.G.E. de Vries, A.K.L. Reyners

Development of methodology: A.R.M. van der Bilt, A.G.T. Terwisscha van Scheltinga, H. Timmer-Bosscha, J.G.W. Kosterink, M.N. Lub-de Hooge, E.G. E. de Vries, A.K.L. Reyners

Acquisition of data (provided animals, acquired and managed patients, provided facilities, etc.): A.R.M. van der Bilt, A.G.T. Terwisscha van Scheltinga, E.G.E. de Vries, A.K.L. Reyners

Analysis and interpretation of data (e.g., statistical analysis, biostatistics, computational analysis): A.R.M. van der Bilt, A.G.T. Terwisscha van Scheltinga, C.P. Schröder, J.G.W. Kosterink, S. de Jong, E.G.E. de Vries, A.K.L. Reyners

Writing, review, and/or revision of the manuscript: A.R.M. van der Bilt, A.G.T. Terwisscha van Scheltinga, H. Timmer-Bosscha, C.P. Schröder, J.G.W. Kosterink, A.G.J. van der Zee, M.N. Lub-de Hooge, S. de Jong, E.G.E. de Vries, A.K.L. Reyners

Administrative, technical, or material support (i.e., reporting or organizing data, constructing databases): A.R.M. van der Bilt, A.G.T. Terwisscha van Scheltinga, L. Pot, A.K.L. Reyners

Study supervision: A.G.T. Terwisscha van Scheltinga, J.G.W. Kosterink, M. N. Lub-de Hooge, E.G.E. de Vries, A.K.L. Reyners

Grant Support

This study was supported by a grant RUG 2010-4603 provided by the Dutch Cancer Society.

The costs of publication of this article were defrayed in part by the payment of page charges. This article must therefore be hereby marked *advertisement* in accordance with 18 U.S.C. Section 1734 solely to indicate this fact.

Received March 14, 2012; revised August 17, 2012; accepted September 16, 2012; published OnlineFirst September 26, 2012.

References

1. Jemal A, Bray F, Center MM, Ferlay J, Ward E, Forman D. Global cancer statistics. CA Cancer J Clin 2011;61:69–90.
2. Burger RA, Brady MF, Bookman MA, Fleming GF, Monk BJ, Huang H, et al. Incorporation of bevacizumab in the primary treatment of ovarian cancer. N Engl J Med 2011;365:2473–83.
3. Perren TJ, Swart AM, Pfisterer J, Ledermann JA, Pujade-Lauraine E, Kristensen G, et al. A phase 3 trial of bevacizumab in ovarian cancer. N Engl J Med 2011;365:2484–96.
4. Altomare DA, Wang HQ, Skele KL, De Rienzo A, Klein-Szanto AJ, Godwin AK, et al. AKT and mTOR phosphorylation is frequently detected in ovarian cancer and can be targeted to disrupt ovarian tumor cell growth. Oncogene 2004;23:5853–7.
5. No JH, Jeon YT, Park IA, Kim YB, Kim JW, Park NH, et al. Activation of mTOR signaling pathway associated with adverse prognostic factors of epithelial ovarian cancer. Gynecol Oncol 2011;121:8–12.
6. Ma XM, Blenis J. Molecular mechanisms of mTOR-mediated translational control. Nat Rev Mol Cell Biol 2009;10:307–18.
7. Skinner HD, Zheng JZ, Fang J, Agani F, Jiang BH. Vascular endothelial growth factor transcriptional activation is mediated by hypoxia-inducible factor 1alpha, HDM2, and p70S6K1 in response to phosphatidylinositol 3-kinase/AKT signaling. J Biol Chem 2004;279:45643–51.
8. Lane HA, Wood JM, McSheehy PM, Allegrini PR, Boulay A, Brueggen J, et al. mTOR inhibitor RAD001 (everolimus) has antiangiogenic/vascular properties distinct from a VEGFR tyrosine kinase inhibitor. Clin Cancer Res 2009;15:1612–22.
9. Mabuchi S, Altomare DA, Connolly DC, Klein-Szanto A, Litwin S, Hoelzle MK, et al. RAD001 (Everolimus) delays tumor onset and progression in a transgenic mouse model of ovarian cancer. Cancer Res 2007;67:2408–13.
10. Mabuchi S, Altomare DA, Cheung M, Zhang L, Poulikakos PI, Hensley HH, et al. RAD001 inhibits human ovarian cancer cell proliferation, enhances cisplatin-induced apoptosis, and prolongs survival in an ovarian cancer model. Clin Cancer Res 2007;13:4261–70.
11. Mabuchi S, Kawase C, Altomare DA, Morishige K, Sawada K, Hayashi M, et al. mTOR is a promising therapeutic target both in cisplatin-sensitive and cisplatin-resistant clear cell carcinoma of the ovary. Clin Cancer Res 2009;15:5404–13.
12. Miyazawa M, Yasuda M, Fujita M, Kajiwara H, Hirabayashi K, Takekoshi S, et al. Therapeutic strategy targeting the mTOR-HIF-1alpha-VEGF pathway in ovarian clear cell adenocarcinoma. Pathol Int 2009;59:19–27.
13. Huynh H, Teo CC, Soo KC. Bevacizumab and rapamycin inhibit tumor growth in peritoneal model of human ovarian cancer. Mol Cancer Ther 2007;6:2959–66.
14. Behbakht K, Sill MW, Darcy KM, Rubin SC, Mannel RS, Waggoner S, et al. Phase II trial of the mTOR inhibitor, temsirolimus and evaluation of circulating tumor cells and tumor biomarkers in persistent and recurrent epithelial ovarian and primary peritoneal malignancies: a Gynecologic Oncology Group study. Gynecol Oncol 2011;123:19–26.
15. Nagengast WB, De Vries EG, Hospers GA, Mulder NH, De Jong JR, Hollema H, et al. *In vivo* VEGF imaging with radiolabeled bevacizumab in a human ovarian tumor xenograft. J Nucl Med 2007;48:1313–9.
16. Nagengast WB, De Korte MA, Oude Munnink TH, Timmer-Bosscha H, Den Dunnen WF, Hollema H, et al. ^{89}Zr-bevacizumab PET of early antiangiogenic tumor response to treatment with HSP90 inhibitor NVP-AUY922. J Nucl Med 2010;51:761–7.
17. Nagengast WB, Lub-De Hooge MN, Oosting SF, Den Dunnen WF, Warnders FJ, Brouwers AH, et al. VEGF-PET imaging is a noninvasive biomarker showing differential changes in the tumor during sunitinib treatment. Cancer Res 2011;71:143–53.
18. Duiker EW, De Vries EG, Mahalingam D, Meersma GJ, Boersma-Van Ek W, Hollema H, et al. Enhanced antitumor efficacy of a DR5-specific TRAIL variant over recombinant human TRAIL in a bioluminescent ovarian cancer xenograft model. Clin Cancer Res 2009;15:2048–57.
19. O'Reilly T, McSheehy PM, Kawai R, Kretz O, McMahon L, Brueggen J, et al. Comparative pharmacokinetics of RAD001 (everolimus) in normal and tumor-bearing rodents. Cancer Chemother Pharmacol 2010;65:625–39.
20. O'Donnell A, Faivre S, Burris HA, Rea D, Papadimitrakopoulou V, Shand N, et al. Phase I pharmacokinetic and pharmacodynamic study of the oral mammalian target of rapamycin inhibitor everolimus in patients with advanced solid tumors. J Clin Oncol 2008;26:1588–95.
21. Honer M, Ebenhan T, Allegrini PR, Ametamey SM, Becquet M, Cannet C, et al. Anti-angiogenic/vascular effects of the mTOR inhibitor everolimus are not detectable by FDG/FLT-PET. Transl Oncol 2010;3:264–75.
22. Cejka D, Kuntner C, Preusser M, Fritzer-Szekeres M, Fueger BJ, Strommer S, et al. FDG uptake is a surrogate marker for defining the optimal biological dose of the mTOR inhibitor everolimus *in vivo*. Br J Cancer 2009;100:1739–45.
23. Bradford MM. A rapid and sensitive method for the quantitation of microgram quantities of protein utilizing the principle of protein-dye binding. Anal Biochem 1976;72:248–54.
24. Duiker EW, Meijer A, Van der Bilt AR, Meersma GJ, Kooi N, Van der Zee AG, et al. Drug-induced caspase 8 upregulation sensitises cisplatin-resistant ovarian carcinoma cells to rhTRAIL-induced apoptosis. Br J Cancer 2011;104:1278–87.
25. Stollman TH, Scheer MG, Leenders WP, Verrijp KC, Soede AC, Oyen WJ, et al. Specific imaging of VEGF-A expression with radiolabeled anti-VEGF monoclonal antibody. Int J Cancer 2008;122:2310–4.
26. Loening AM, Gambhir SS. AMIDE: a free software tool for multimodality medical image analysis. Mol Imaging 2003;2:131–7.
27. Gershenson DM. The heterogeneity of epithelial ovarian cancer: getting it right. Cancer 2010;116:1400–2.
28. Gourley C, Michie CO, Keating KE, Deharo S, O'Brien EJ, Winter A, et al. Establishing a molecular taxonomy for epithelial ovarian cancer (EOC) from 363 formalin-fixed paraffin embedded (FFPE) specimens. J Clin Oncol 29: 2011 (suppl; abstr 5000).
29. Tanaka C, O'Reilly T, Kovarik JM, Shand N, Hazell K, Judson I, et al. Identifying optimal biologic doses of everolimus (RAD001) in patients with cancer based on the modeling of preclinical and clinical pharmacokinetic and pharmacodynamic data. J Clin Oncol 2008;26:1596–602.
30. Baker AF, Dragovich T, Ihle NT, Williams R, Fenoglio-Preiser C, Powis G. Stability of phosphoprotein as a biological marker of tumor signaling. Clin Cancer Res 2005;11:4338–40.
31. Ma WW, Jacene H, Song D, Vilardell F, Messersmith WA, Laheru D, et al. (18F)fluorodeoxyglucose positron emission tomography correlates with Akt pathway activity but is not predictive of clinical outcome during mTOR inhibitor therapy. J Clin Oncol 2009;27:2697–704.

32. Kinross KM, Brown DV, Kleinschmidt M, Jackson S, Christensen J, Cullinane C, et al. *In vivo* activity of combined PI3K/mTOR and MEK inhibition in a KrasG12D;Pten deletion mouse model of ovarian cancer. Mol Cancer Ther 2011;10:1440–9.
33. Wei LH, Su H, Hildebrandt IJ, Phelps ME, Czernin J, Weber WA. Changes in tumor metabolism as readout for mammalian target of rapamycin kinase inhibition by rapamycin in glioblastoma. Clin Cancer Res 2008;14:3416–26.
34. Stollman TH, Scheer MG, Franssen GM, Verrijp KN, Oyen WJ, Ruers TJ, et al. Tumor accumulation of radiolabeled bevacizumab due to targeting of cell- and matrix-associated VEGF-A isoforms. Cancer Biother Radiopharm 2009;24:195–200.
35. Oosting SF, Nagengast WB, Oude Munnink TH, Lub-De Hooge MN, Brouwers AH, Glaudemans AWJM, et al. ^{89}Zr-bevacizumab PET imaging in renal cell carcinoma patients: feasibility of tumor VEGF quantification. Eur J Cancer Suppl 2010;8:72–3.
36. Paez-Ribes M, Allen E, Hudock J, Takeda T, Okuyama H, Vinals F, et al. Antiangiogenic therapy elicits malignant progression of tumors to increased local invasion and distant metastasis. Cancer Cell 2009; 15:220–31.